



**HAL**  
open science

## Thermal evolution of hydrated asteroids inferred from oxygen isotopes

Lionel Vacher, Maxime Piralla, Matthieu Gounelle, Martin Bizzarro, Yves Marrocchi

► **To cite this version:**

Lionel Vacher, Maxime Piralla, Matthieu Gounelle, Martin Bizzarro, Yves Marrocchi. Thermal evolution of hydrated asteroids inferred from oxygen isotopes. *The Astrophysical journal letters*, 2019, 882, pp.L20. 10.3847/2041-8213/ab3bd0 . hal-02331795

**HAL Id: hal-02331795**

**<https://hal.univ-lorraine.fr/hal-02331795>**

Submitted on 24 Oct 2019

**HAL** is a multi-disciplinary open access archive for the deposit and dissemination of scientific research documents, whether they are published or not. The documents may come from teaching and research institutions in France or abroad, or from public or private research centers.

L'archive ouverte pluridisciplinaire **HAL**, est destinée au dépôt et à la diffusion de documents scientifiques de niveau recherche, publiés ou non, émanant des établissements d'enseignement et de recherche français ou étrangers, des laboratoires publics ou privés.



Distributed under a Creative Commons Attribution 4.0 International License

1 **Thermal evolution of hydrated asteroids inferred from oxygen isotopes**

2  
3  
4  
5 Lionel G. Vacher<sup>1,2,\*</sup>, Maxime Piralla<sup>1</sup>, Matthieu Gounelle<sup>3</sup>, Martin Bizzarro<sup>4</sup> & Yves  
6 Marrocchi<sup>1</sup>

7  
8  
9 <sup>1</sup>CRPG, CNRS, Université de Lorraine, UMR 7358, Vandoeuvre les Nancy, F-54501, France

10  
11 <sup>2</sup>Department of Physics, Washington University, St. Louis, MO, USA

12  
13 <sup>3</sup>IMPMC, MNHN, UPMC, UMR CNRS 7590, 61 rue Buffon, 75005 Paris, France

14  
15 <sup>4</sup>Centre for Star and Planet Formation and Natural History Museum of Denmark, University  
16 of Copenhagen, DK-1350 Copenhagen, Denmark

17  
18 \* corresponding author: l.vacher@wustl.edu

19  
20  
21  
22  
23  
24  
25  
26  
27  
28  
29  
30  
31  
32  
33  
34  
35  
36  
37  
38  
39  
40  
41  
42  
43  
44  
45  
46  
47  
48  
49  
50  
51  
52

53           **Abstract**

54

55           Chondrites are fragments of unmelted asteroids that formed due to gravitational  
56 instabilities in turbulent regions of the Solar protoplanetary disk. Hydrated chondrites are  
57 common among meteorites, indicating that a substantial fraction of the rocky bodies that  
58 formed early in the Solar System accreted water ice grains that subsequently melted due to  
59 heat released by the radioactive decay of  $^{26}\text{Al}$ . However, the thermal histories of asteroids are  
60 still largely unknown whereas it would bring fundamental information on their timing of  
61 accretion and their physical characteristics. Here we show that hydrated meteorites (CM  
62 chondrites) contain previously uncharacterized calcium carbonates with peculiar oxygen  
63 isotopic compositions ( $\Delta^{17}\text{O} \approx -2.5 \text{‰}$ ), which artificially produce the mass-independent trend  
64 previously reported for carbonates. Based on these isotopic data, we propose a new model to  
65 quantitatively estimate the precipitation temperatures of secondary phases (carbonates and  
66 serpentine). It reveals that chondritic secondary phases recorded a gradual increase of the  
67 temperature during the extent of aqueous alteration, from  $-10 \text{ °C}$  to maximum  $250 \text{ °C}$ . We  
68 also show that the thermal path of C-type asteroids is independent of the initial oxygen  
69 isotopic composition of the primordial water ice grains that they accreted. Our estimated  
70 temperatures for hydrated asteroids remain lower than those experienced by other  
71 carbonaceous chondrites, providing strong constraints for modelling the formation conditions  
72 and size-distribution of water-rich asteroids, especially in anticipation of the return of samples  
73 of water-rich asteroids to Earth by the OSIRIS-REx and Hayabusa2 missions.

74 **1. Introduction**

75

76 Dark C-type asteroids dominate the main-belt asteroid population and are genetically  
77 related to hydrous primitive CI and CM carbonaceous chondrites (Vilas & Gaffey 1989; Hiroi  
78 et al. 1996; Vilas 1994; Burbine et al. 2002; Lauretta et al. 2019). CM chondrites are the most  
79 common water-rich meteorites, and CM-like matter represent an important fraction of  
80 exogenic clasts reported in other groups of meteorites, implying that CM parent bodies are  
81 widespread in the asteroid belt (Briani et al. 2012). CM chondrites are complex aggregates of  
82 high-temperature components formed in the disk and low-temperature secondary minerals  
83 formed during subsequent parent-body fluid circulations. The latter provide key constraints  
84 on the origin of water accreted by asteroids (Vacher et al. 2016; Piani et al. 2018) as well as  
85 their accretion and evolution histories (Young et al. 2003; Verdier-Paoletti et al. 2017; Vacher  
86 et al. 2017; Fujiya et al. 2015). CM chondrites are therefore important samples because they  
87 show varying degrees of alteration that can be easily estimated by their chemical alteration  
88 index (Rubin et al. 2007; Marrocchi et al. 2014; Vacher et al. 2018). Among secondary  
89 minerals, carbonates are of primary importance as they represent direct proxies of the  
90 asteroidal fluids from which they formed and can, in theory, be used to decipher their thermal  
91 evolution (Clayton & Mayeda 1984). However, determining carbonate precipitation  
92 temperatures requires knowledge of the O isotopic compositions of their parental fluids,  
93 which itself requires knowledge of the carbonate precipitation temperatures, leading to a  
94 seemingly circular problem.

95 The temperature of CM carbonate precipitation remains largely underconstrained and  
96 proposed values cover a large range of temperatures. More generally, the sequence of  
97 formation of the different secondary phases (carbonates, serpentine) is poorly understood.  
98 Based on ‘clumped-isotopes’ and oxygen isotopic analyses, it has been proposed that CM

99 carbonates could have precipitated at both low and medium temperatures, in the range of 0-  
100 75°C (Clayton & Mayeda 1984; Benedix et al. 2003; Guo & Eiler 2007) and 50-350°C  
101 (Verdier-Paoletti et al. 2017; Alexander et al. 2015). However, these two different  
102 methodologies do not take account the petrographic relationship between carbonates and  
103 serpentine (Fuchs et al. 1973; Zolensky et al. 1997; Brearley 2006; Rubin et al. 2007; Vacher  
104 et al. 2018; Lee et al. 2013; 2014), which can constrain the evolution of the fluid over time. In  
105 addition, different types of carbonates are present in CM chondrites (Vacher et al. 2017; Lee  
106 et al. 2013; 2014) but no specific attention has been paid on their respective oxygen isotopic  
107 compositions. The objectives of this paper are thus to determine the oxygen isotopic  
108 composition of petrographically characterized carbonates in order to quantify the thermal  
109 evolution of hydrated asteroids. To do so, we surveyed a suite of different CM chondrites  
110 characterized by varying degrees of alteration: CM2.6/2.7 Maribo (van Kooten et al. 2018),  
111 CM2.5 Murchison (Rubin et al. 2007), CM2.4/2.7 Jbilet Winselwan (King et al. 2018) and  
112 CM2.0 Mukundpura (Rudraswami et al. 2018). Based on oxygen isotopic compositions of  
113 carbonates, we propose a new isotopic alteration model that reconciles petrographic  
114 observations and formation temperatures of CM carbonates.

115

## 116 **2. Material and methods**

### 117 *2.1 SEM imaging*

118 Calcite grains were located in carbon coated (i) polished sections of Murchison,  
119 Mukundpura and Jbilet Winselwan (samples provided by the Muséum National d'Histoire  
120 Naturelle in Paris) and (ii) thin section of Maribo (section provided by the Natural History  
121 Museum of Denmark in Copenhagen) using a Scanning Electron Microscope (SEM) JEOL  
122 JSM-6510 equipped with an energy dispersive X-ray detector (Bruker-AXS XFlash, silicon  
123 drift detector) at Centre de Recherches Pétrographiques et Géochimiques (CRPG, Nancy,

124 France). Back-Scattered Electron (BSE) imaging were performed with a 3 nA electron beam  
125 current operated at 15 kV.

126

## 127 *2.2 SIMS oxygen isotope analyses of calcite*

128 Calcite oxygen isotopic compositions were analysed using a CAMECA IMS 1270 E7 at  
129 CRPG laboratory. A Cs<sup>+</sup> primary ion beam (~15x10 μm spot area) with a current of ~5 nA  
130 was used in order to collect <sup>16</sup>O<sup>-</sup>, <sup>17</sup>O<sup>-</sup> and <sup>18</sup>O<sup>-</sup> secondary ions in multi-collection mode using  
131 three Faraday cups (L'2, FC2 and H1). Charge compensation was applied using a normal-  
132 incidence electron gun. Mass Resolving Power (MRP = M/ΔM) was adjusted to ~7000 to  
133 resolve interference from <sup>16</sup>OH<sup>-</sup> on the <sup>17</sup>O<sup>-</sup> peak and achieve maximum flatness on the top of  
134 the <sup>16</sup>O<sup>-</sup> and <sup>18</sup>O<sup>-</sup> peaks (entrance and exit slits of FC2 were adjusted to ~70 μm and ~170 μm,  
135 respectively). <sup>16</sup>O<sup>-</sup> and <sup>18</sup>O<sup>-</sup> secondary ions were collected on L'2 and H1, respectively (slit 1,  
136 MRP ≈ 2500). Pre-sputter on a large area (~20x20 μm) was applied before each measurement  
137 during 60s in order to remove carbon coating at the surface of the calcite grains. Acquisition  
138 time was set to ~5s and measurements were repeated over 30 cycles to achieve counting  
139 statistics ~0.2‰ (1σ) for δ<sup>18</sup>O and ~0.3‰ for δ<sup>17</sup>O. Isotope ratios (<sup>17</sup>O/<sup>16</sup>O and <sup>18</sup>O/<sup>16</sup>O) are  
140 presented in per mil (‰) relative to Standard Mean Ocean Water (SMOW):

$$141 \quad \delta^x\text{O}_{SMOW}(\text{‰}) = \left( \frac{x\text{O}/^{16}\text{O}_{sample}}{x\text{O}/^{16}\text{O}_{SMOW}} - 1 \right) \times 1000 \quad (1)$$

142 where  $x$  represents <sup>17</sup>O or <sup>18</sup>O and SMOW the ratios of the SMOW standard. We measured  
143 two in-house terrestrial standards to define the Terrestrial Fractionation Line (TFL): (i) quartz  
144 (SiO<sub>2</sub>) from Brazil (δ<sup>18</sup>O = 9.6‰, <sup>16</sup>O = 2 × 10<sup>9</sup> cps and <sup>18</sup>O = 4.2 × 10<sup>6</sup> cps) and (ii) calcite  
145 (CaCO<sub>3</sub>) from Mexico (δ<sup>18</sup>O = 23.6‰, <sup>16</sup>O = 2 × 10<sup>9</sup> cps and <sup>18</sup>O = 4.2 × 10<sup>6</sup> cps; 0.03 wt% of  
146 MgO). Instrumental Mass Fractionation (IMF) for calcite matrix was determined from our in-  
147 house Mexican calcite standard at the beginning and end of each analytical session. IMF  
148 values for each sample analysis were then calculated by accounting for the linear deviation

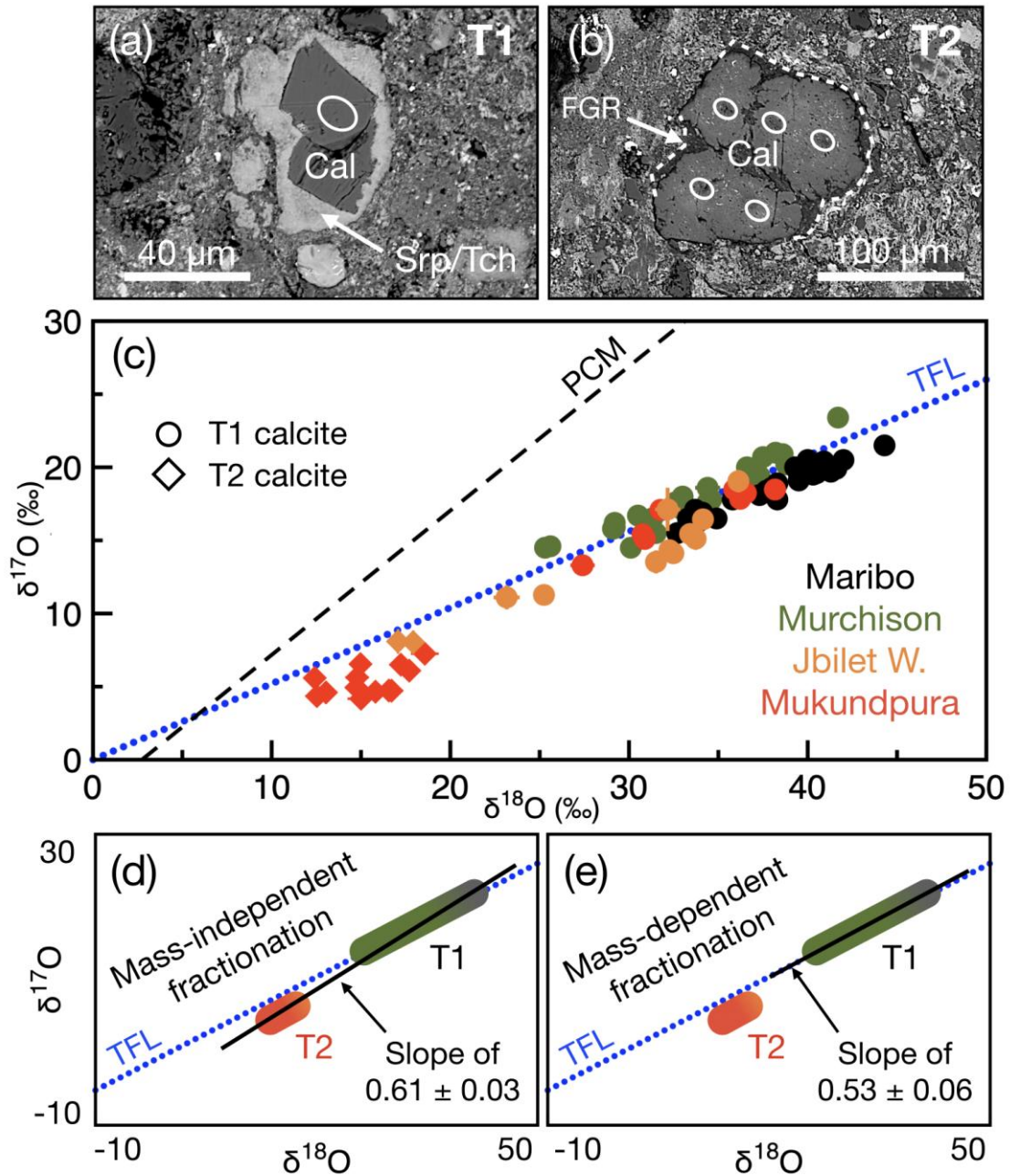
149 over the time of the IMF values. Typical measurement errors ( $2\sigma$ ), accounting for errors on  
150 each measurement and the external reproducibility of the standard, were estimated to be  
151  $\sim 0.5\text{‰}$  for  $\delta^{18}\text{O}$ ,  $\sim 0.6\text{‰}$  for  $\delta^{17}\text{O}$ , and  $\sim 0.7\text{‰}$  for  $\Delta^{17}\text{O}$  (i.e.,  $\Delta^{17}\text{O} = \delta^{17}\text{O} - 0.52 \times \delta^{18}\text{O}$ ),  
152 where  $\Delta^{17}\text{O}$  represents the departure from the TFL.

153

### 154 **3. Results**

155

156 In the four CM chondrites surveyed in this work, calcite grains surrounded by Fe-S-  
157 rich serpentine/tochilinite (hereafter T1 calcite; Fig. 1a) are ubiquitous whereas serpentine-  
158 free polycrystalline calcite grains containing Fe-Ni sulfide inclusions (hereafter T2 calcite;  
159 Fig. 1b) have only been observed in two sections (Jbilet Winselwan and Mukundpura). The O  
160 isotopic compositions of T1 calcite grains measured herein vary widely, with  $\delta^{18}\text{O}$  values  
161 ranging from 23.1 to 44.3‰,  $\delta^{17}\text{O}$  from 11.1 to 23.4‰ and  $\Delta^{17}\text{O}$  from  $-2.8$  to  $+1.8\text{‰}$  (Figs 1c  
162 & S1, Table S1), whereas T2 calcite grains have homogeneous compositions with  $\delta^{18}\text{O}$  values  
163 ranging from 12.6 to 18.4‰,  $\delta^{17}\text{O}$  from 4.2 to 8.1‰ and  $\Delta^{17}\text{O}$  from  $-4$  to  $-0.8\text{‰}$  (Figs 1c &  
164 S1, Table S2)



165

166 **Fig. 1:** Backscattered electron images of (a) a T1 calcite grain (Cal) surrounded by a Fe-S-rich  
 167 Serpentine/Tochilinite rim (Srp/Tch) in the matrix of Murchison and (b) a T2 calcite grain that is free of  
 168 serpentine/tochilinite rim, but is instead surrounded by a rim of Fine-Grained Matrix (FGR; white dashed  
 169 line) in the matrix of Mukundpura. White circles represent the locations of SIMS analytical spots. (c)  $\delta^{17}\text{O}$ -  
 170  $\delta^{18}\text{O}$  plot for T1 (circles) and T2 (diamonds) calcites from the CM chondrites Maribo (black), Murchison  
 171 (green), Jbilet Winselwan (orange) and Mukundpura (red) ( $2\sigma$  errors). Schematic  $\delta^{17}\text{O}$ - $\delta^{18}\text{O}$  diagrams  
 172 represent the linear correlations (black solid lines) obtained considering (d) T1 and T2 calcites, defining a  
 173 mass-independent trend with a slope of  $0.61 \pm 0.03$  and (e) only T1 calcites, defining a mass-dependent  
 174 trend with a slope of  $0.53 \pm 0.06$ . TFL = Terrestrial Fractionation Line ( $\delta^{17}\text{O} = 0.52 \times \delta^{18}\text{O}$ ); PCM =  
 175 Primary Chondrule Minerals line ( $\delta^{17}\text{O} = 0.987 \times \delta^{18}\text{O} - 2.7$ ).



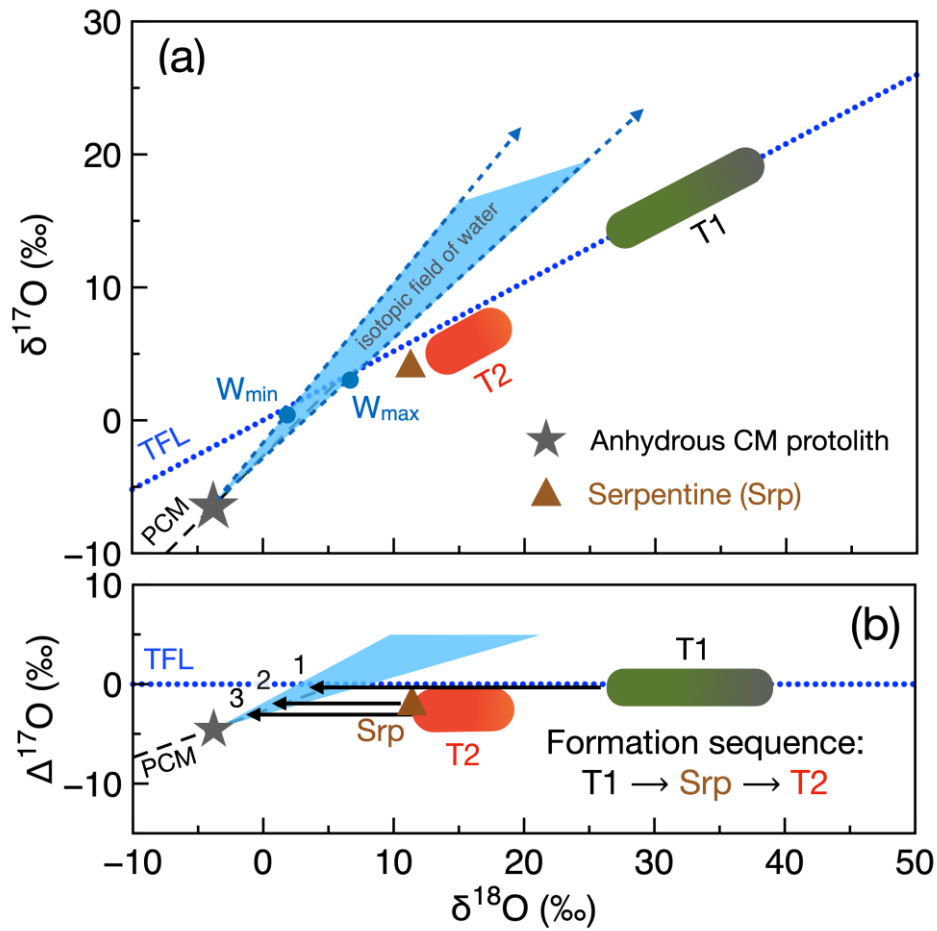
#### 176 4. Discussion

177

178 Together, T1 and T2 calcite grains define a mass-independent trend with  $\delta^{17}\text{O} = (0.61$   
179  $\pm 0.03) \times \delta^{18}\text{O} - (3.3 \pm 1.1)$  (Fig. 1c–d) that is similar, within errors, to those commonly  
180 reported in different CM chondrites (Vacher et al. 2018). As a first approximation, this trend  
181 suggests that the O isotopic compositions of CM carbonates is essentially controlled by  
182 variable degrees of isotopic exchanges between  $^{16}\text{O}$ -rich anhydrous silicates and a  $^{17,18}\text{O}$ -rich  
183 fluid (Fig. 1d; Verdier-Paoletti et al. 2017; Marrocchi et al. 2018). However, the O isotopic  
184 compositions of T1 calcites alone define a distinct trend with  $\delta^{17}\text{O} = (0.53 \pm 0.06) \times \delta^{18}\text{O} -$   
185  $(1.2 \pm 2.2)$  that is indistinguishable, within errors, from the TFL (i.e.,  $\Delta^{17}\text{O} = -0.4 \pm 1.0$ ; Fig.  
186 1e). Conversely, T2 calcites exhibit clustered  $\delta^{17}\text{O} - \delta^{18}\text{O}$  values (Figs 1c & S1, Table S2)  
187 with  $\Delta^{17}\text{O} = -2.6 \pm 1.0$ , which artificially produce the aforementioned mass-independent  
188 trend when taken together with T1 calcites (Fig. 1d). This demonstrates that petrographic  
189 observations of carbonates are essential for understanding the O isotopic evolution of  
190 asteroidal fluids and the constraints they bear.

191 Based on mass-balance calculations, tentative attempts at estimating the O isotopic  
192 composition of primordial water accreted by CM chondrites have led to widely ranging and  
193 contrasted results due to assumptions on the O isotopic composition of the anhydrous  
194 protolith and asteroidal thermal evolution ( $\delta^{18}\text{O}_{\text{fluid}} = 16\text{--}55\text{‰}$ ,  $\delta^{17}\text{O}_{\text{fluid}} = 9\text{--}35\text{‰}$  and  
195  $\Delta^{17}\text{O}_{\text{fluid}} = 0.9\text{--}6.6\text{‰}$ ; Verdier-Paoletti et al. 2017; Clayton & Mayeda 1999; Fujiya 2018).  
196 However, these values correspond to the initial water composition and do not represent the  
197 oxygen isotopic compositions of fluids from which carbonates precipitated, which had Earth-  
198 like compositions with  $\Delta^{17}\text{O} \approx 0\text{‰}$  (Fig. 1c; Vacher et al. 2016; Verdier-Paoletti et al. 2017).  
199 Quantitative estimates of the O isotopic compositions of the parental fluids of carbonates have  
200 been obtained by  $\text{CO}_2$  clumped-isotope thermometry ( $\Delta^{47}$ ; Guo & Eiler 2007), which

201 corresponds to anomalous enrichments of mass 47 (i.e.,  $^{13}\text{C}^{18}\text{O}^{16}\text{O}$ ) in  $\text{CO}_2$  derived from  
202  $\text{H}_3\text{PO}_4$  digestion of carbonates (Ghosh et al. 2006). Based on measurements performed on the  
203 CM chondrites Murchison and Murray, dominated by T1 calcites, Guo & Eiler (2007)  
204 estimated that the O isotopic compositions of their alteration fluids ranged from  $\delta^{18}\text{O} = 2\text{‰}$   
205 and  $\Delta^{17}\text{O} = -0.6\text{‰}$  (hereafter  $W_{\text{min}}$ ; Fig. 2a) to  $\delta^{18}\text{O} = 6.8\text{‰}$  and  $\Delta^{17}\text{O} = -0.5\text{‰}$  (hereafter  
206  $W_{\text{max}}$ ; Fig. 2a). Because these fluids experienced oxygen isotopic exchanges with the  
207 anhydrous CM chondrite protolith ( $\delta^{18}\text{O} = -3.8\text{‰}$ ,  $\delta^{17}\text{O} = -6.5\text{‰}$ ; Fig. S2), they define two  
208 trends that delimit the possible O isotopic compositions of CM alteration fluids (blue shaded  
209 area in Fig. 2a). Considering these extreme trends, the precipitation temperatures of each T1  
210 calcite grain can be calculated according to the isotopic fractionation factor  $\alpha$  (Watkins et al.  
211 2013), which corresponds to the distance between the minimum and maximum trends and the  
212 O isotopic compositions of carbonates in the three oxygen isotope diagram. This estimation  
213 leads to respective minimum ( $T_{\text{min}}$ ) and maximum ( $T_{\text{max}}$ ) precipitation temperatures of  $-9 \pm$   
214  $11 \text{ °C}$  and  $5 \pm 14 \text{ °C}$  for Maribo,  $19 \pm 22 \text{ °C}$  and  $50 \pm 34 \text{ °C}$  for Murchison,  $15 \pm 21 \text{ °C}$  and  $33$   
215  $\pm 29 \text{ °C}$  for Jbilet Winselwan and  $12 \pm 17 \text{ °C}$  and  $34 \pm 22 \text{ °C}$  for Mukundpura ( $1\sigma$ ; Table 1  
216 and Fig. 3a). On average, this gives minimum and maximum precipitation temperatures for all  
217 T1 calcites of  $7 \pm 22 \text{ °C}$  and  $29 \pm 32 \text{ °C}$ , respectively ( $1\sigma$ ).



218

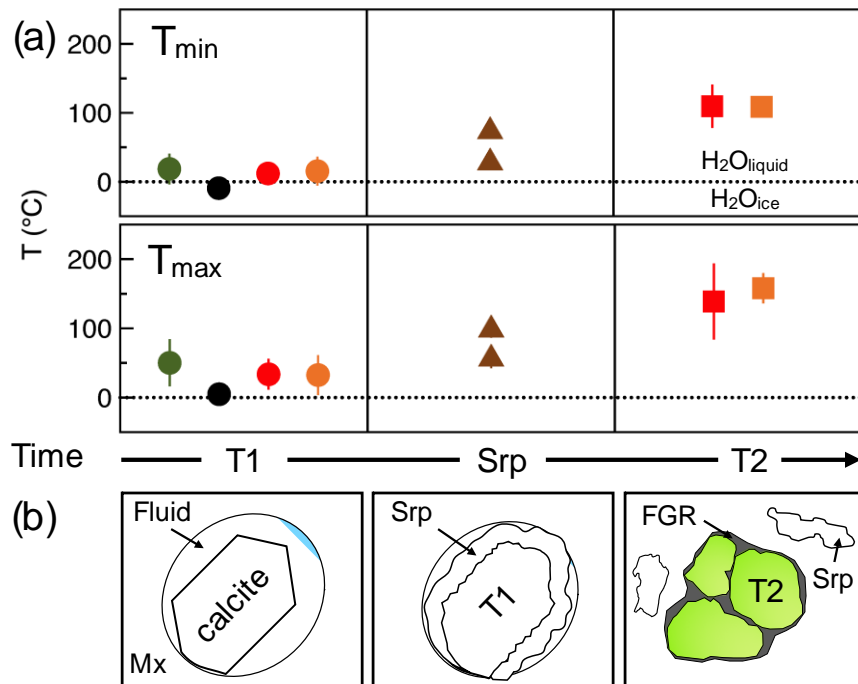
219 **Fig. 2:** (a)  $\delta^{17}\text{O}$ - $\delta^{18}\text{O}$  plot showing simplified ranges for T1 and T2 calcites, the mean bulk value of CM  
 220 serpentine (Srp, brown triangle) and the isotopic field of CM water (blue shaded area) as determined from  
 221 the isotopic equilibration (blue dashed lines) of the minimum ( $W_{\min}$ ) and maximum ( $W_{\max}$ ) compositions of  
 222 the parental water of T1 calcites (blue circles) with the anhydrous CM protolith (grey star; see  
 223 Supplementary Fig. S1 for details). (b)  $\delta^{18}\text{O}$ - $\Delta^{17}\text{O}$  plot showing the isotopic equilibration of CM water with  
 224 the anhydrous CM protolith. In this diagram, mass-dependent isotopic fractionations plot on a horizontal  
 225 line. The decrease of the mean  $\Delta^{17}\text{O}$  values of the secondary phases ( $\Delta^{17}\text{O}_{\text{T1}} = 0.4\text{‰}$ ,  $\Delta^{17}\text{O}_{\text{Srp}} = -2.2\text{‰}$  and  
 226  $\Delta^{17}\text{O}_{\text{T2}} = -2.4\text{‰}$ ; see Supplementary Tables S1 and S2 and Clayton & Mayeda 1999) indicates the  
 227 following formation sequence: (1) T1 calcites, (2) serpentines and (3) T2 calcites.

228

229 **Table 1:** Mean O isotopic compositions of secondary phases and their calculated minimum ( $T_{\min}$ ) and  
 230 maximum ( $T_{\max}$ ) formation temperatures (O'Neil et al., 1969). Uncertainties are  $1\sigma$ .  
 231

Meteorite	Petrologic subtype	Secondary phase	Sample number	Mean $\delta^{18}\text{O}$ (‰)	Mean $\Delta^{17}\text{O}$ (‰)	Mean $T_{\min}$ (°C)	Mean $T_{\max}$ (°C)
Maribo	CM2.6/2.7 <sup>a</sup>	T1 calcite	25	38.3 ( $\pm 3.1$ )	-1.2 ( $\pm 0.5$ )	-9 ( $\pm 11$ )	5 ( $\pm 14$ )
Murchison	CM2.5 <sup>b</sup>	T1 calcite	24	33.7 ( $\pm 4.5$ )	0.4 ( $\pm 0.8$ )	19 ( $\pm 22$ )	50 ( $\pm 34$ )
Jbilet	CM2.4/2.7 <sup>c</sup>	T1 calcite	10	31.4 ( $\pm 4.1$ )	-1.6 ( $\pm 1.2$ )	15 ( $\pm 21$ )	33 ( $\pm 29$ )
Winselwan		T2 calcite	2	17.5 ( $\pm 0.6$ )	-1 ( $\pm 0.3$ )	109 ( $\pm 11$ )	158 ( $\pm 22$ )
Mukundpura	CM2.0 <sup>d</sup>	T1 calcite	8	33.5 ( $\pm 3.8$ )	-0.7 ( $\pm 0.6$ )	12 ( $\pm 17$ )	34 ( $\pm 22$ )
		T2 calcite	13	15.4 ( $\pm 2$ )	-2.6 ( $\pm 1$ )	110 ( $\pm 32$ )	139 ( $\pm 55$ )
Bulk CM	–	Serpentine <sup>e</sup>	5	11.7 ( $\pm 0.6$ )	-2.2 ( $\pm 0.3$ )	28 ( $\pm 8$ ) <sup>f</sup> 73 ( $\pm 7$ ) <sup>g</sup>	56 ( $\pm 13$ ) <sup>f</sup> 98 ( $\pm 11$ ) <sup>g</sup>

232 References: <sup>a</sup>(van Kooten et al. 2018); <sup>b</sup>(Rubin et al. 2007); <sup>c</sup>(King et al. 2018); <sup>d</sup>(Rudraswami  
 233 et al. 2018); <sup>e</sup>(Clayton & Mayeda 1999); <sup>f</sup>(Früh-Green et al. 1996); <sup>g</sup>(Zheng 1993)  
 234



235  
 236 **Fig. 3:** (a) Minimum ( $T_{\min}$ ) and maximum ( $T_{\max}$ ) precipitation temperatures of T1 calcites (circles),  
 237 serpentines (brown triangles) and T2 calcites (diamonds) calculated as a function of their formation  
 238 sequence/time (errors are  $1\sigma$ ) using previously reported fractionation factors for calcite (O'Neil et al.,  
 239 1969) and serpentine (Früh-Green et al. 1996; Zheng 1993). Colours are as in Fig. 1. (b) Schematic  
 240 representation of the formation sequence of (1) T1 calcite, (2) serpentine around T1 calcite and (3) T2  
 241 calcite, as deduced from petrographic observations and the mean  $\Delta^{17}\text{O}$  values of these three phases (see  
 242 Fig. 2c).  
 243

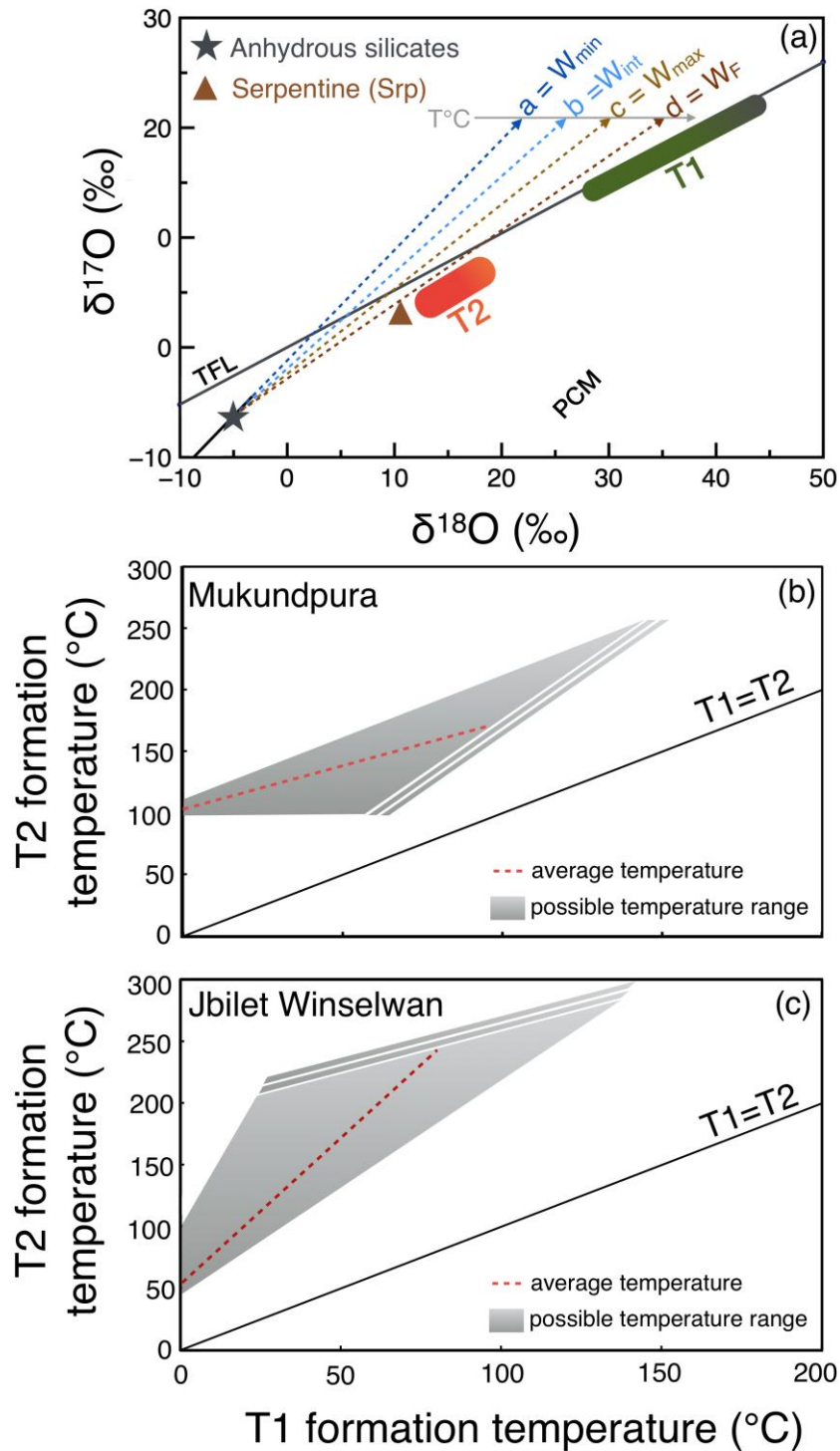
244 The large range of  $\delta^{17}\text{O}$ - $\delta^{18}\text{O}$  values and constant  $\Delta^{17}\text{O}$  values observed in T1 calcites  
245 (Fig. 1c–e, Table S1) imply that T1 calcites precipitated along a temperature gradient from  
246 alteration fluids characterized by a fixed  $\Delta^{17}\text{O}$  value. On the other hand, T2 calcites (this  
247 study) and serpentine (Clayton & Mayeda 1984) formed from a more  $^{16}\text{O}$ -rich fluid that  
248 resulted from protracted isotopic exchange with the  $^{16}\text{O}$ -rich anhydrous protolith and thus  
249 evolved toward negative  $\Delta^{17}\text{O}$  values (Fig. 2b). Following the same methodology as for T1  
250 calcites, we calculated the formation temperatures of T2 calcites to be significantly higher,  
251 with respective minimum and maximum temperatures being  $109 \pm 11$  °C and  $158 \pm 22$  °C for  
252 Jbilet Winselwan and  $110 \pm 11$  °C and  $139 \pm 55$  °C for Mukundpura ( $1\sigma$ ; Table 1 and Fig.  
253 3a); respective average values are  $109 \pm 29$  °C and  $141^\circ\text{C} \pm 52^\circ\text{C}$  ( $1\sigma$ ). The same calculation  
254 for bulk serpentine compositions ( $n = 5$ ; Clayton & Mayeda 1999) gives minimum and  
255 maximum formation temperatures of  $28 \pm 8$  to  $56 \pm 13$  °C and  $73 \pm 7$  to  $98 \pm 11$  °C,  
256 respectively, depending of the fractionation factor considered (Früh-Green et al. 1996; Zheng  
257 1993;  $1\sigma$ ; Table 1 and Fig. 3a).

258 Our petrographic and isotopic approaches reveal that T1 calcites precipitated at lower  
259 temperatures than serpentines and T2 calcites (Fig. 3a). These results support petrographic  
260 observations suggesting that T2 calcites correspond to a later stage of alteration, as  
261 highlighted by (i) the absence of serpentine rims and (ii) the existence of a fine-grained rim  
262 (FGR) suggesting that they replaced chondrule silicates (Fig. 3b; Lee et al. 2014; Lindgren et  
263 al. 2017). This implies that fluid circulation in CM parent bodies, and thus the formation of  
264 CM secondary phases, occurred during a prograde thermal evolution (Figs. 2b and 3b; Vacher  
265 et al. 2019), with T1 calcites forming first at  $T = -10$  to  $+50$  °C, followed by the precipitation  
266 of (Fe,S)-rich serpentine (mostly cronstedtite; Pignatelli et al. 2016; 2017) and tochilinite at  $T$   
267  $= 30$ – $100$  °C and finally T2 calcites at  $T = 110$ – $160$  °C (Fig. 3a, Table 1).

268 According to X-ray diffraction studies (Howard et al. 2011; 2009), serpentine  
269 represent the most abundant mineral in CM chondrites (75 vol% in average). Their formations  
270 (posterior to that of T1 calcites) would thus affect the isotopic evolution of the alteration  
271 fluids, leading to a slight shift toward  $^{16}\text{O}$ -enriched values. As this isotopic shift is not taken  
272 into account in our model, this implies that the precipitation temperatures estimated for T2  
273 calcites (Fig. 3a, Table 1) should be considered as maximum values. However, as the  
274 fractionation factor  $\alpha$  is significantly lower for serpentine-water than for calcite-water (i.e.,  
275  $1000\ln\alpha_{\text{serpentine-water}} = 6.3$  vs  $1000\ln\alpha_{\text{calcite-water}} = 17.1$  at  $100^\circ\text{C}$ ; O'Neil et al. 1969; Fruh-  
276 Green et al., 1996), this approximation does not affect our main conclusions that T1 calcites  
277 precipitated at lower temperature than T2 calcites.

278 As the uncertainties on the O isotopic compositions of primordial water accreted by  
279 CM chondrites could also affect our conclusions, we tested our results with different initial O  
280 isotopic compositions (Fig. 4). According to the currently favoured self-shielding model,  
281 primordial water is hypothesized to have had a large  $^{17,18}\text{O}$  enrichment (i.e.,  $\delta^{17}\text{O} = \delta^{18}\text{O} \approx$   
282  $180\%$ ; Sakamoto et al. 2007) plotting on a line of slope 1 in a three oxygen isotope diagram.  
283 However, mass balance calculations performed on the O isotopic compositions of CM  
284 chondrites at bulk and mineral scales suggest more modest enrichments in the heavy oxygen  
285 isotopes with  $\delta^{17}\text{O} = 35 \pm 9\%$  and  $\delta^{18}\text{O} = 55 \pm 13\%$  (Fujiya 2018). Hence, we tested our  
286 results by using primordial CM water O isotopic compositions corresponding to (i) a  
287 composition intermediate between  $W_{\min}$  and  $W_{\max}$  ( $W_{\text{int}}$ ) and (ii) the values proposed by  
288 Fujiya (2018) ( $W_{\text{F}}$ , Fig. 4a). Isotopic exchange between these fluid compositions and the  
289 anhydrous CM protolith (Marrocchi et al. 2018) thus defines two other lines on the  $\delta^{17,18}\text{O}$   
290 diagram (b and d in Fig. 4a, with lines a and c corresponding to the trends defined by  $W_{\min}$   
291 and  $W_{\max}$ , respectively) from which the precipitation temperatures of T1 and T2 calcites can  
292 be calculated according to the fractionation factor  $\alpha$  (Watkins et al. 2013). The results for

293 Jbilet Winselwan and Mukundpura (the only meteorites containing T2 calcites in this study)  
294 systematically show that T2 calcites precipitated at higher temperatures than T1 calcites (Fig.  
295 4b–c), regardless of the oxygen isotopic composition used for primordial water. Depending  
296 on the isotopic trend considered (a, b, c or d in Fig. 4a), the average precipitation temperatures  
297 of T1 calcites range from 10 to 100 °C, whereas T2 calcites formed between 110 and 245 °C  
298 (Fig. 4b–c). We note that the absolute temperatures at which secondary phases formed is  
299 directly affected by the oxygen isotopic composition of primordial chondritic water, whose  
300 precise determination is thus fundamental to better quantifying the thermal evolution of  
301 hydrated asteroids.



302

303 **Fig. 4:** (a)  $\delta^{17}\text{O}$ - $\delta^{18}\text{O}$  plot showing the four trends (see text) used to calculate the influence of the initial  
 304 oxygen isotopic composition of primordial water on the thermal path interpreted for water-rich asteroids.  
 305 (b, c)  $\delta^{17}\text{O}$ - $\delta^{18}\text{O}$  plots showing the results of the model for Mukundpura and Jbilet Winselwan, respectively.  
 306 In both cases, the average formation temperatures of T2 calcites are systematically higher than those  
 307 estimated for T1 calcites (red dashed lines), even when accounting for variability in the  $\delta^{17}\text{O}$  and  $\delta^{18}\text{O}$   
 308 values of calcites in Jbilet Winselwan and Mukundpura (grey triangles).

309



310 Another possible source of uncertainty in estimating precipitation temperatures arises  
311 if T1 calcites experienced post-precipitation isotopic reequilibration, especially if CM  
312 chondrites experienced peak temperatures as high as 250 °C. However, this appears unlikely  
313 as T1 calcites systematically show mass-dependent oxygen isotopic variations  
314 (Supplementary Fig. S3), whereas isotopic exchange between initial water and anhydrous  
315 silicates during reequilibration would have induced  $\Delta^{17}\text{O}$  variations (Fig. 2a). In addition,  
316 according to the values of oxygen self-diffusion in calcite (Anderson 2007; Farver 1994), 1–  
317  $10^4$  Gyr are required to isotopically reequilibrate calcite grains of 5 $\mu\text{m}$  in size at temperatures  
318  $\leq 200$  °C (Fig. S3). Such results thus strengthen our conclusion that hydrated asteroids  
319 experienced a prograde thermal evolution with T1 calcites precipitating first, followed by  
320 serpentine and then T2 calcites.

321 By taking into account the petrographic type of carbonates, our hydrothermal  
322 temperature estimates for CM chondrites are higher than previously proposed (Clayton &  
323 Mayeda 1984; Benedix et al. 2003; Guo & Eiler 2007) but remain low ( $< 250$  °C) compared to  
324 the peak of thermal metamorphism experienced by other groups of carbonaceous chondrites,  
325 such as CO or CV chondrites (up to 500–600 °C; Bonal et al. 2007; Busemann et al. 2007;  
326 Cody et al. 2008; Ganino & Libourel 2017). This implies the relatively late accretion of  
327 water-rich asteroids in the protoplanetary disk, as water-poor asteroids that accreted earlier  
328 experienced significantly higher temperatures due to the radioactive decay of  $^{26}\text{Al}$ . Based on  
329  $\epsilon^{54}\text{Cr}$  anomalies, it has been proposed that CM chondrites accreted  $\sim 3.7$ – $5.0$  Myr after the  
330 formation of CV calcium-aluminium-rich inclusions (CAIs; Fujiya et al. 2012; Doyle et al.  
331 2015; Sugiura & Fujiya 2014), after a five-fold decrease in the abundance of  $^{26}\text{Al}$ , whereas  
332 CO and CV chondrites accreted  $\sim 2.1$ – $2.4$  and  $\sim 2.4$ – $2.6$  Myr after CV CAIs, respectively  
333 (Doyle et al. 2015). Interestingly, recent spectral data provided by the Osiris-REx and  
334 Hayabusa2 asteroid sample return missions suggest that C-type asteroid Ryugu has

335 experienced more heating than B-type asteroid Bennu (Hamilton et al. 2019; Kitazato et al.,  
336 2019). Although late shock heating could have induced such features, their different thermal  
337 history could also be the result of distinct accretion ages. The returned samples from Osiris-  
338 REx and Hayabusa2 in the near future will likely contain hydrated minerals (Kitazato et al.  
339 2019; Lauretta et al. 2019) whose *in-situ* isotopic analyses would provide information on the  
340 thermal alteration processes and formation histories of asteroids Ryugu and Bennu.

341

## 342 **5. Conclusions**

343

344 In this letter, we report the results of *in-situ* oxygen isotope analyses performed on  
345 alteration phases (calcium carbonates) from a suite of different hydrated meteorites (CM  
346 chondrites) to quantitatively estimate the thermal evolution of hydrated asteroids. Based on our  
347 isotopic results, we propose a new isotopic model that reconciles formation temperatures and  
348 petrographic observations of secondary minerals whose isotopic compositions recorded a  
349 gradual increase of the temperature (up to 250°C) during a prograde evolution of the  
350 temperature, regardless the oxygen isotopic composition of the initial water. These results are  
351 fundamental because they imply that hydrated asteroids accreted relatively late in the  
352 protoplanetary disk, as their earlier accretion would have led to higher alteration temperatures  
353 due to higher concentrations of radioactive  $^{26}\text{Al}$ . Although more precise radioactive dating  
354 and numerical modelling are required, our study provides a key method to quantitatively  
355 estimate the respective thermal histories of the asteroids Bennu (Lauretta et al. 2019) and  
356 Ryugu (Sugita et al. 2019; Watanabe et al. 2019) upon the return of samples to Earth.

357

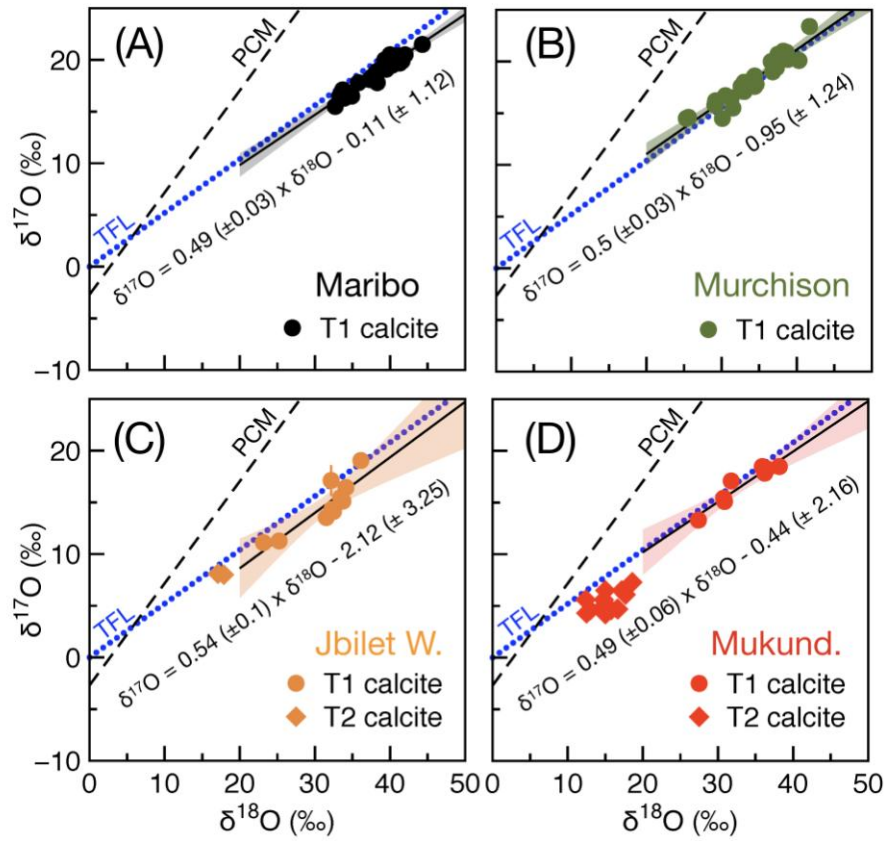
358

## 359 **Acknowledgments**

360

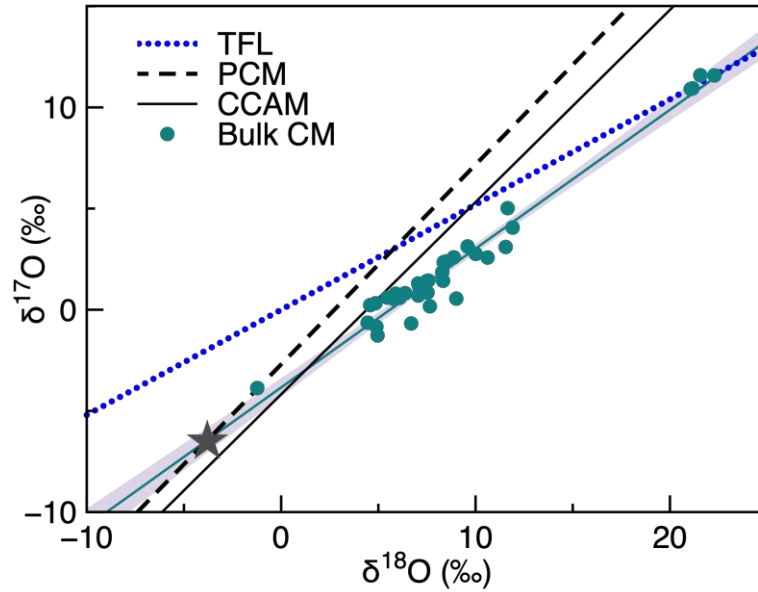
361 The authors are grateful to Nordine Bouden and Johan Villeneuve for their assistance  
362 with the isotopic measurements. Laurette Piani is thanked for helpful scientific discussions.

363 The Muséum National d'Histoire Naturelle (Paris) and The Natural History Museum of  
364 Denmark (Copenhagen) are also thanked for providing samples of Mukundpura and sections  
365 of Maribo chondrites. We thank Pr. Frederic Rasio for his editorial handling and the  
366 anonymous reviewer for his comments that contributed to improve the quality of the  
367 manuscript. This research was funded by l'Agence Nationale de la Recherche through grant  
368 ANR-587 14-CE33-0002-01 SAPINS (PI Yves Marrocchi). This is CRPG contribution #2714.  
369



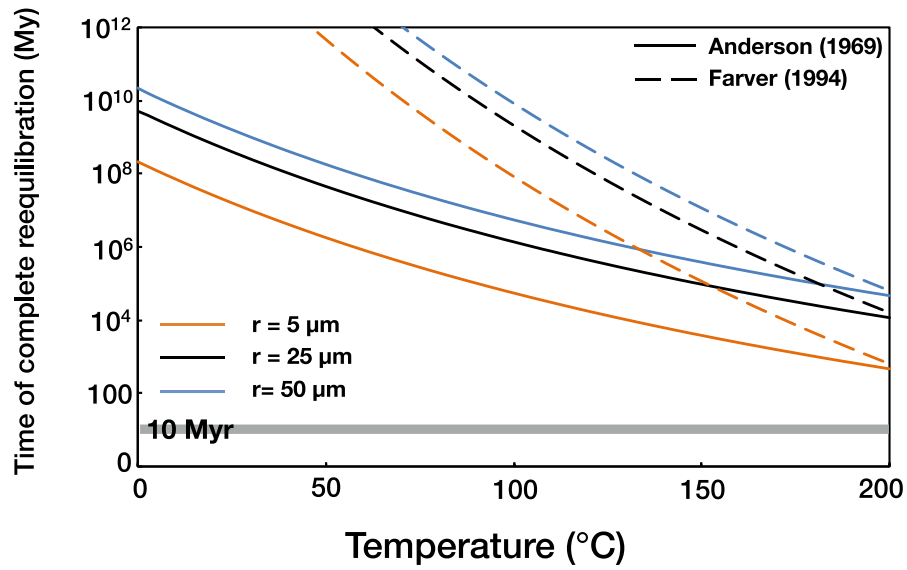
372  
 373 **Fig. S1:**  $\delta^{17}\text{O}$ - $\delta^{18}\text{O}$  plots showing the mass-dependent trends (black solid line) defined by T1 calcites  
 374 (circles) for each CM chondrite: (a) Maribo, (b) Murchison, (c) Jbilet Winselwan and (d) Mukundpura.  
 375 Shaded areas represent the 95% confidence interval for each slope. T2 calcites (diamonds) are also shown  
 376 for Jbilet Winselwan (c) and Mukundpura (d), the only chondrites studied herein containing T2 calcites.  
 377 Errors are  $2\sigma$ .

378  
 379  
 380  
 381  
 382



383  
 384 **Fig. S2:**  $\delta^{17}\text{O}$ - $\delta^{18}\text{O}$  plot showing the O isotopic composition of the anhydrous CM protolith (i.e., the  
 385 theoretical anhydrous bulk CM composition:  $\delta^{18}\text{O} = -3.8\text{‰}$  and  $\delta^{17}\text{O} = -6.5\text{‰}$ ; grey star) determined from  
 386 the linear correlation of the CM bulk composition (green circle (Clayton & Mayeda 1999; Hewins et al.  
 387 2014)). The anhydrous CM protolith corresponds to the intercept between the bulk CM trend ( $\delta^{17}\text{O} = 0.69$   
 388  $\times \delta^{18}\text{O} - 3.8$ ;  $n = 36$ ) and the PCM line ( $\delta^{17}\text{O} = 0.987 \times \delta^{18}\text{O} - 2.7$ ; (Ushikubo et al. 2012)). CCAM:  
 389 Carbonaceous chondrite anhydrous minerals line.

390  
 391  
 392  
 393  
 394  
 395  
 396  
 397  
 398



399  
 400  
 401  
 402  
 403  
 404  
 405  
 406  
 407  
 408  
 409  
 410  
 411  
 412  
 413  
 414  
 415  
 416  
 417  
 418  
 419  
 420  
 421  
 422  
 423

**Fig. S3:** Time (Myr) required for the complete reequilibration of early precipitated T1 calcite as a function of grain size (radius) and temperature, calculated using oxygen self-diffusion parameters for calcite (Farver 1994). The grey shaded region at 10 Myr corresponds to the duration estimated for fluid circulations in asteroidal parent bodies (Fujiya et al. 2012; Doyle et al. 2015; Petit et al. 2011).

**Table S1:** Oxygen isotopic compositions of T1 calcite grains in the CM chondrites Maribo, Murchison, Jbilet Winselwan and Mukundpura.

#	$\delta^{18}\text{O}$	$2\sigma$	$\delta^{17}\text{O}$	$2\sigma$	$\Delta^{17}\text{O}$	$2\sigma$
CC7	32.7	0.3	15.5	0.5	-1.5	0.8
CC21-1	33.3	0.3	16.5	0.8	-0.8	1
CC21-2	33.9	0.3	16.3	0.7	-1.3	0.9
CC22	33.7	0.3	17.1	0.5	-0.4	0.8
CC20	34.1	0.4	16.9	0.6	-0.9	0.9
CC27	34.9	0.2	16.5	0.5	-1.7	0.7
CC30	35.8	0.3	17.8	0.5	-0.8	0.7
CC10	37.3	0.6	18.1	0.6	-1.3	1
CC11	37.7	0.2	18.4	0.5	-1.3	0.7
CC4-2	38	0.3	18.6	0.5	-1.1	0.8
CC4-1	41.6	0.3	19.9	0.5	-1.7	0.7
CC5	38.3	0.3	18.9	0.6	-1.1	0.8
CC17	38.3	0.3	17.8	0.6	-2.2	0.8
CC9	39.3	0.3	20	0.5	-0.4	0.8
CC33	39.5	0.3	19.1	0.5	-1.4	0.5
CC32	39.5	0.3	19.6	0.7	-0.9	0.9
CC13	40	0.5	20.5	0.6	-0.3	1
CC3	40.2	0.3	20	0.6	-0.9	0.7
CC28	40.3	0.2	19.5	0.6	-1.4	0.8
CC29	40.5	0.3	19.6	0.6	-1.5	0.6
CC12	40.6	0.3	19.7	0.5	-1.4	0.8
CC15	40.9	0.4	20.4	0.5	-0.9	0.6
CC2	41.3	0.3	19.7	0.5	-1.7	0.8
CC18	42	0.3	20.5	0.5	-1.4	0.8
CC1	44.3	0.3	21.5	0.6	-1.5	0.8
<b>Mean</b>	<b>38.3</b>		<b>18.7</b>		<b>-1.2</b>	
<i>StDev</i>	<i>3.1</i>		<i>1.6</i>		<i>0.5</i>	
CC-7-2	25.3	0.2	14.5	0.4	1.3	0.3
CC-7-3	25.6	0.2	14.6	0.4	1.3	0.4
A-CC-5-2	29.1	0.5	15.8	0.4	0.7	0.6
A-CC-5-3	36.6	0.2	20	0.3	1	0.3
A-CC-8-2	29.2	0.6	15.9	0.6	0.7	0.7
CC-1-2	29.2	0.3	16.2	0.4	1	0.4
A-CC-11-1	30.1	0.5	14.5	0.6	-1.1	0.7
CC-6	30.5	0.3	16.7	0.3	0.8	0.4
A-CC-3-2	31.3	0.9	16.5	0.8	0.3	1.1
A-CC-3-1	34.4	0.7	18.6	0.7	0.7	0.9
A-CC-10	31.5	0.9	15.5	0.6	-0.9	1.0
A-CC-13	32.6	0.3	17.6	0.3	0.7	0.4
A-CC-7	33	0.5	17.1	0.6	0	0.7
CC-18	33	0.2	18	0.3	0.9	0.3
A-CC-2-2	34.4	0.6	17.6	0.6	-0.3	0.8
CC-3	34.6	0.3	17.8	0.4	-0.2	0.4
CC-2	36.8	0.2	19	0.3	-0.1	0.3
CC-5	37.3	0.6	19.4	0.6	0	0.8
CC-10	37.5	0.2	20.7	0.3	1.2	0.3
CC-12	38.2	0.3	21	0.3	1.1	0.3
A-CC-1	38.6	0.6	20.9	0.6	0.8	0.8
CC-11	38.8	0.3	20.2	0.3	0	0.4
CC-9	40.3	0.3	20.1	0.3	-0.8	0.4
CC-8	41.7	0.4	23.4	0.3	1.8	0.4
<b>Mean</b>	<b>33.7</b>		<b>18</b>		<b>0.4</b>	
<i>StDev</i>	<i>4.5</i>		<i>2.4</i>		<i>0.8</i>	
CC-6	23.1	0.7	11.1	0.8	-0.9	1.0
CC-5	25.2	0.4	11.3	0.7	-1.9	0.7
CC-11	31.5	0.5	13.5	0.8	-2.8	0.9

CC-3	32.2	0.7	17.1	1.5	0.4	1.6
CC-2	32.3	0.6	14.3	0.7	-2.4	0.8
CC-7	32.5	0.5	14.1	0.7	-2.8	0.7
CC-9	33.4	0.5	15.4	0.7	-1.9	0.7
CC-8	33.7	0.5	15.1	0.8	-2.4	0.8
CC-1	34.1	0.5	16.4	0.7	-1.3	0.8
CC-10	36.1	0.5	19.1	0.8	0.3	0.8
<b>Mean</b>	<b>31.4</b>		<b>14.8</b>		<b>-1.6</b>	
<i>StDev</i>	<i>4.1</i>		<i>2.5</i>		<i>1.2</i>	
CC15	27.4	0.7	13.3	0.4	-0.9	0.6
CC13	30.8	0.6	15.4	0.4	-0.6	0.6
CC14	30.9	0.6	15.1	0.4	-1	0.6
CC1	31.8	0.5	17.1	0.4	0.6	0.5
CC12	35.9	0.6	18.5	0.4	-0.2	0.6
CC8-1	36.2	0.6	17.8	0.4	-1	0.6
CC11	36.5	0.6	18.2	0.4	-0.8	0.6
CC7-1	38.2	0.6	18.5	0.4	-1.4	0.6
<b>Mean</b>	<b>33.5</b>		<b>16.7</b>		<b>-0.7</b>	
<i>StDev</i>	<i>3.8</i>		<i>1.9</i>		<i>0.6</i>	

Shaded rows denote multiple analyses of the same grain.

426  
427  
428  
429  
430  
431  
432  
433  
434  
435  
436  
437  
438  
439  
440  
441  
442  
443  
444  
445  
446  
447  
448  
449  
450  
451  
452  
453  
454  
455  
456  
457  
458  
459  
460



461 **Table S2:** Oxygen isotopic compositions of T2 calcite grains in the CM chondrites Jbilet Winselwan and  
 462 Mukundpura.

#	$\delta^{18}\text{O}$	$2\sigma$	$\delta^{17}\text{O}$	$2\sigma$	$\Delta^{17}\text{O}$	$2\sigma$
CC15	17.1	0.4	8.1	0.9	-0.8	0.9
CC14	17.9	0.5	8	0.8	-1.3	0.0
<b>Mean</b>	<b>17.5</b>		<b>8.1</b>		<b>-1</b>	
<i>StDev</i>	<i>0.6</i>		<i>0</i>		<i>0.3</i>	
CC3-1	12.4	0.6	5.6	0.3	-0.9	0.5
CC3-4	12.5	0.6	4.3	0.4	-2.2	0.6
CC3-3	13	0.6	4.6	0.4	-2.2	0.6
CC3-2	15	0.5	6.5	0.4	-1.2	0.6
CC17-1	14.7	0.6	4.9	0.4	-2.7	0.6
CC17-2	17.7	0.6	6.1	0.4	-3.1	0.6
CC5-1	14.8	0.7	5.6	0.4	-2	0.6
CC5-5	15	0.8	4.2	0.5	-3.6	0.7
CC5-3	15.8	0.7	4.6	0.4	-3.6	0.7
CC5-2	16.6	0.5	4.7	0.4	-3.9	0.5
CC5-4	16.7	0.6	4.7	0.5	-4	0.6
CC6-1	17.2	0.6	6.5	0.4	-2.5	0.6
CC9	18.6	0.8	7.3	0.4	-2.4	0.7
<b>Mean</b>	<b>15.4</b>		<b>5.4</b>		<b>-2.6</b>	
<i>StDev</i>	<i>2.0</i>		<i>1.0</i>		<i>1.0</i>	

Shaded rows denote multiple analyses of the same grain.

463  
 464  
 465  
 466  
 467  
 468  
 469  
 470  
 471  
 472  
 473  
 474  
 475  
 476  
 477  
 478  
 479  
 480  
 481  
 482  
 483  
 484  
 485  
 486  
 487  
 488  
 489  
 490  
 491  
 492  
 493

494 **References**

- 495 Alexander, C. M. O., Bowden, R., Fogel, M. L., & Howard, K. T. 2015, MPS, 50, 810.
- 496 Anderson, T. F. 1969, J. Geophys. Res., 74, 3918.
- 497 Benedix, G. K., Leshin, L. A., Farquhar, J., Jackson, T., et al 2003, GCA, 67, 1577.
- 498 Bonal, L., Bourot-Denise, M., Quirico, E., et al. 2007, GCA, 71, 1605.
- 499 Brearley, A. J. 2006, MESS II, 943, 587.
- 500 Briani, G., Gounelle, M., Bourot-Denise, M., & Zolensky, M. E. 2012, MPS, 47, 880.
- 501 Burbine, T., McCoy, T., Meibom, A., Gladman, B., & Keil, K. 2002, Asteroids III, 1, 653.
- 502 Busemann, H., Alexander, C. M. O'D., & Nittler, L. R. 2007, MPS, 42, 1387.
- 503 Clayton, R. N., & Mayeda, T. K. 1984, EPSL, 67, 151.
- 504 Clayton, R. N., & Mayeda, T. K. 1999, GCA, 63, 2089.
- 505 Cody, G. D., Alexander, C. M. O'D., Yabuta, H., et al. 2008, EPSL, 272, 446.
- 506 Doyle, P.M., Jogo, K., Nagashima, K., et al. 2015, Nat Comms 6, 7444.
- 507 Farver, J.R. 1994, EPSL, 121, 575.
- 508 Früh-Green, G. L., Plas, A, Lécuyer C. 1996, 14. *Proc. Ocean Drilling. Programm.* 147, 255.
- 509 Fuchs, L. H., Olsen, E., & Jensen, K. J. 1973, Smithsonian Contr. Earth Sci., 10, 1.
- 510 Fujiya, W., Sugiura, N., Hotta, H., et al. 2012, Nat Comms, 3, 627.
- 511 Fujiya, W., Sugiura, N., Marrocchi, Y., et al. 2015, GCA, 161, 101.
- 512 Fujiya, W. 2018, EPSL, 481, 264.
- 513 Ganino, C., Libourel, G. 2017 Nat Comms, 8, 261.
- 514 Ghosh, P., Adkins, J., Affek, H., et al. 2006, GCA, 70, 1349.
- 515 Guo, W., & Eiler, J. M. 2007, GCA, 71, 5565.
- 516 Hamilton, V. E., Simon, A. A., Christensen, P. R., et al. 2019, Nat. Astron., 3, 332.
- 517 Hewins, R. H., Bourot-Denise, M., Zanda, B., et al. 2014, GCA, 124, 190.
- 518 Hiroi, T., Pieters, C. M., Zolensky, M. E., & Lipschutz, M. E. 1996, MPS, 31, 321.
- 519 Howard, K. T., Benedix, G. K., Bland, P. A., & Cressey, G. 2009, GCA, 73, 4576.
- 520 Howard, K. T., Benedix, G. K., Bland, P. A., & Cressey, G. 2011, GCA, 75, 2735.
- 521 King, A. J., Russell, S. S., Schofield, P. F., et al. 2018, MPS, 49, 62.
- 522 Kitazato, K, Milliken, R. E., Iwata, T., et al. 2019, Science, 364, 272.
- 523 Lauretta D.S., DellaGiustina, D. N., Bennett, C. A., et al. 2019, Nature, 568, 55.
- 524 Lee, M. R., Sofe, M. R., Lindgren, P., Starkey, N. A., & Franchi, I. A. 2013, GCA, 121, 452.
- 525 Lee, M. R., Lindgren, P., & Sofe, M. R. 2014, GCA, 144, 126.
- 526 Lindgren, P., Lee, M. R., Starkey, N. A., Franchi, I. A. 2017, GCA, 204, 240.
- 527 Marrocchi, Y., Gounelle, M., Blanchard, I., et al., 2014, MPS, 49, 1232.
- 528 Marrocchi, Y., Bekaert, D. V., & Piani, L. 2018, EPSL, 482, 23.
- 529 O'Neil, J.R., Clayton, R.N. & Mayeda, T.K. 1969, J. Chem. Phys. 51, 5547.
- 530 Petitat, M., Marrocchi, Y., McKeegan, K. D., et al. 2011, MPS, 46, 275.
- 531 Piani, L., Yurimoto, H., & Remusat, L. 2018, Nat. Astron. 2, 317.
- 532 Pignatelli, I., Marrocchi, Y., Mugnaioli, E., et al. 2017, GCA, 209, 106.
- 533 Pignatelli, I., Marrocchi, Y., Vacher, et al. 2016, MPS, 51, 785.
- 534 Rubin, A. E., Trigo-Rodriguez, J. M., & Huber, H. 2007, GCA, 71, 2361.
- 535 Rudraswami, N. G., Naik, A. K., Tripathi, R. P., et al. 2018, Geoscience Frontiers, 1-10.
- 536 Sakamoto, N., Seto, Y., Itoh, S., et al. 2007, Science, 317, 231.
- 537 Sugita, S., Tatsumi, E., Okada, T., et al. 2019, Science, 364, eaaw0422.
- 538 Sugiura, N., Fujiya, W. 2014, MPS, 49, 772.
- 539 Ushikubo, T., Kimura, M., Kita, N. T., Valley, J. W. 2012, GCA, 90, 242.
- 540 Vacher, L. G., Marrocchi, Y., Verdier-Paoletti, M. J., Villeneuve, J., & Gounelle, M., 2016, ApJ L, 827, L1-6.
- 542 Vacher, L. G., Marrocchi, Y., Villeneuve, J., Verdier-Paoletti, M. J., & Gounelle, M., 2017, GCA, 213, 271.
- 543

- 544 Vacher, L. G., Marrocchi, Y., Villeneuve, J., Verdier-Paoletti, M. J., & Gounelle, M.,2018,  
545 GCA, 239, 213.
- 546 Vacher, L. G., Truche, L., Faure, F., et al. 2019, MPS, 23, 237.
- 547 van Kooten, E. M. M. E., Cavalcante, L. L., Nagashima, K., et al. 2018, GCA, 79, 102.
- 548 Verdier-Paoletti, M. J., Marrocchi, Y., Avice, G., et al. 2017, EPSL, 458, 273.
- 549 Vilas, F. 1994, Icarus, 111, 456.
- 550 Vilas, F., & Gaffey, M. J. 1989, Science, 246, 790.
- 551 Watanabe, S., Hirabayashi, M., Hirata, N., et al 2019, Science, 364, 26.
- 552 Watkins, J. M., Nielsen, L. C., Ryerson, F. J., & DePaolo, D. J. 2013, EPSL, 375, 349.
- 553 Young, E. D., Zhang, K. K., & Schubert, G. 2003, EPSL, 213, 249.
- 554 Zolensky, M. E., Mittlefehldt, D. W., Lipschutz, M. E., et al. 1997, GCA, 61, 5099.
- 555 Zheng Y.-F. 1993, GCA, 57, 1079.